This is a non-final version of an article published in final form in Exp Neurol 2021 Feb;336:113533. doi: 10.1016/j.expneurol.2020.113533. Epub 2020 Nov 29

# Lumbar perineuronal nets preservation by voluntary wheel running prevents hyperreflexia and enhances motor function after SCI

**Authors**

Sanchez-Ventura J[1], Giménez-Llort L[2], Penas C[1], Udina E[1*]

**Affiliation**

[1]Institute of Neurosciences, Department Cell Biology, Physiology and Immunology, Universitat Autònoma de Barcelona, and Centro de Investigación Biomédica en Red sobre Enfermedades Neurodegenerativas (CIBERNED), Bellaterra, Spain

[2]Institute of Neurosciences, Department of Psychiatry and Forensic Medicine, Universitat Autònoma de Barcelona, Bellaterra, Spain.

**Correspondence**:

* esther.udina@uab.cat; Telf: +34935811348

## Abstract

Perineuronal nets (PNN) are a promising candidate to harness neural plasticity, favoring the stabilization of circuits at expenses of plasticity. Interestingly, physical activity reduces encephalic PNN, enhancing plasticity, but it increases spinal PNN. Due to the relevance of rehabilitation treatments after spinal cord injuries (SCI), it is important to better understand how spinal PNN are affected in these injuries and their impact on spinal circuits. Thus, this work aims to describe PNN alterations after thoracic SCI in mice, followed by different types of activity-dependent therapies: enriched environment, voluntary wheel and forced treadmill running. We found that the contusion provoked thermal hyperalgesia, hyperreflexia and locomotor impairment as measured by thermal plantar test, H wave recordings and the BMS score of locomotion, respectively. SCI reduced the density of PNN around lumbar motoneurons. In contrast, activity-based therapies increased motoneuron activity and reversed lumbar PNN decrease after SCI. Interestingly, the voluntary wheel group showed full preservation of PNN which also correlated with reduced hyperreflexia and a better locomotor recovery. Furthermore, both voluntary wheel and treadmill running reduced hyperalgesia, but this finding was independent of lumbar PNN levels. The results of the present study highlight the impact of SCI on decreasing PNN at caudal segments of the spinal cord and the potential of physical activity-based therapies to reverse PNN disaggregation and to improve functional recovery. Altogether, since modulating plasticity is crucial for restoring the function of the damaged neural circuits, regulating PNN by activity is an encouraging target to improve the outcome after injury.

*Keywords:* spinal cord injury, perineuronal nets, motoneurons, physical activity, hyperreflexia, neuropathic pain.

## Introduction

One of the hallmarks of the central nervous system (CNS) is its potential to maintain the right balance between plasticity and stability. While plasticity prevails during development, stability predominates in the adult nervous system (1). This fine plastic control is mediated, in part, by perineuronal nets (PNN). PNN are an aggregation of extracellular matrix molecules, among them chondroitin sulphate proteoglycans (CSPG), with open gaps that regulate synaptic contacts (2). Their appearance temporally correlates with the maturation of the central synaptic circuitry and determines the end of the critical periods (3). As a dynamic structure, these nets are subjected to an activity-dependent modulation. Hence, physical activity increases plasticity by means of reducing cerebellar (4) and cortical PNN (5). On the contrary, recent studies have pointed out that activity increases PNN around spinal motoneurons (5,6) and thus, it jeopardizes the statement that activity always increases plasticity in the nervous system. Therefore, activity seems to differently modulate PNN depending on the anatomical localization (5). Understanding how physical activity or exercise regulates spinal PNN can have a huge impact, especially on spinal cord injury (SCI) models, since physical rehabilitation is currently one of the cornerstones for the treatment of SCI in humans.

SCI leads to devastating and non-reversible functional deficits due to the limited ability of central neurons to regenerate after injury. One main factor contributing to this regenerative failure is the upregulation of CSPGs (7). In fact, the application of chondroitinase ABC (chABC), an enzyme that degrades proteoglycans, at the injury site (8) or in distal regions where proteoglycans were also overexpressed (9,10), promoted functional recovery. Despite an apparent contradiction, the combination of ChABC treatment with specific rehabilitation further enhances functional recovery after injury, even if the applied rehabilitation increases the density of PNN (11,12). Thus, although spinal proteoglycan degradation is a potential strategy to boost plasticity, any approach must be mindful of plasticity-stability trade-off. In fact, maladaptive plastic changes can lead to the appearance of neuropathic pain and spasticity after SCI. Interestingly, physical exercise can attenuate both phenomena in experimental models of SCI (13,14).

In the spinal cord, PNN are mainly found around lower motoneurons (15). Therefore, it is important to specifically evaluate the fate of spinal PNN after SCI, besides the generalized increase of proteoglycans related to reactive astrocytes (7). It is also worth pointing that despite their mesh-like appearance and their inhibitory role, their negatively charged net generates a microenvironment around neurons that contributes to the fine-tuning of neuron function regulating ionic buffering, neuroprotection, synaptic stabilization and neuronal development and plasticity (*reviewed in* (16,17)*)*.

Therefore, an optimal understanding of how spinal PNN are modulated after SCI and which is the influence of activity-dependent therapies on these nets is still needed. The present study aims to

evaluate the changes that lumbar PNN surrounding spinal motoneurons suffer after a thoracic SCI, and also its effects on PNN of the dorsal column nuclei in the brainstem. We hypothesized that reduced physical activity after a thoracic SCI would decrease PNN thickness around lumbar motoneurons, facilitating the disorganization of the circuitry, whereas the opposite effect would be observed in PNN of the sensory brain stem nuclei. Activity-dependent therapies might reverse those effects on PNN, through activating sensory and motor output and segmental reflexes such as the stretch reflex. To address these hypotheses, we used a contusion SCI in mice that were subjected to three different types of physical activities: an enriched environment, a voluntary and a forced exercise (*Figure 1*).

## RESULTS

### Voluntary wheel running enhances functional recovery after SCI

Locomotor function, evaluated as the Basso Mouse Scale (BMS) score, is shown in *Figure 2A*. All injured animals presented impaired hindlimb locomotion just after the injury and then, a gradual recovery during the following weeks. Only mice that voluntary run on the wheel (WR) showed significant improvement of BMS score at 28 and 35 dpi compared to the sedentary (SED) group or to the group of animals forced to run in a treadmill (TR) (WR: 4.43 ± 0.13 *vs*. SED: 3.30 ± 0.12 ($p<0.001$) and TR: 3.60 ± 0.19 ($p<0.05$) at 28 dpi, WR: 4.64 ± 0.09 *vs.* SED: 3.4 ± 0.19 ($p<0.001$) and TR: 3.6 ± 0.19 at 35 dpi ($p<0.01$)). In the WR group, the improvements of BMS score over time were also statistically significant ($p<0.001$). Despite the enriched environment (EE) group slightly increased the BMS score and a trend over time was observed, they did not reach statistical significance (EE: 3.71 ± 0.29 at 28dpi and 4 ± 0.18 at 35 dpi).

The results of the thermal algesimetry tests (*Figure 2B*) indicated that all SCI groups developed thermal hyperalgesia at 14 dpi as shown by a significant decrease in the withdrawal latency compared to the control intact group (SED 0.62 ± 0.07 ($p<0.001$); EE 0.67 ± 0.14 ($p<0.01$); WR 0.69 ± 0.10 ($p<0.01$); TR 0.75 ± 0.05 ($p<0.05$) *vs.* CTRL 1.03 ± 0.05). At later time points, whereas the SED and EE groups maintained low threshold (SED 0.62 ± 0.08 ($p<0.01$); EE 0.57 ± 0.08 ($p<0.001$) *vs.* CTRL), the WR and TR groups increased their withdrawal latency towards control values (WR 0.765 ± 0.096; TR 0.871 ± 0.068). *Figure 2C* shows that the percentage of animals with thermal hyperalgesia at 28 dpi was considerably higher in the SED group than in the activity-treated groups (SED: 87.5%; EE: 66.67%; WR: 42.86%; TR: 37.5%).

The electrophysiological tests performed before SCI showed that motor evoked potentials (MEPs) elicited by brain stimulation were present in all mice (data not shown). Contrarily, six days after contusion, MEPs were abolished in the hindlimb muscles of all injured animals (*Figure 2D*). MEPs reappeared during the follow-up, but recovery was different in the three tested muscles. In the plantar and tibialis anterior muscles, the WR and EE groups presented a percentage of recovery higher than the SED and TR groups at the end of the experiment (Plantar muscle: EE: 36.56 ± 10.95; vs SED: 7.02 ± 6.37 ($p<0.05$) and TR: 9.52 ± 5.65 ($p<0.05$); WR: 42.33 ± 13.53 vs SED ($p<0.01$) and TR ($p<0.01$); Tibialis anterior muscle: EE: 68.40 ± 12.71 vs SED: 27.79 ± 9.24 ($p<0.001$); TR: 25.43 ± 5.21 ($p<0.001$) and WR: 54.77 ± 2.08 vs SED ($p<0.01$) and TR ($p<0.001$)). However, in the gastrocnemius muscle, this increased recovery was only observed in the EE group compared to the rest of groups (EE: 43.1 ± 7.15 vs WR: 26.57 ± 2.81 ($p<0.01$), TR: 34.82 ± 5.43 ($p<0.05$), SED: 17.81 ± 3.4 ($p<0.001$)). Altogether, these results indicate that the EE and WR groups presented a higher recuperation of supraspinal connections during the follow-up. However, we did not find increased white matter preservation in 1.2 mm around the epicenter of the injury in the EE nor WR groups as compared to the rest (*Figure Suppl2).*

Regarding the H reflex (*Figure 2E*), control animals did not show noticeable changes in their $H_{max}/M_{max}$ ratio during the follow-up (CTRL: 0.18 ± 0.01, 0.17 ± 0.02 and 0.19 ± 0.01 at 6, 21 and 32 dpi respectively), whereas the SCI produced hyperreflexia in 72% of the animals at 6 dpi (data not shown). At 21 and 32 dpi, $H_{max}/M_{max}$ ratio was maintained at similar levels than at 6dpi in all the injured groups except the WR group, in which presented a significant decrease over time (WR: 0.53 ± 0.04, 0.41 ± 0.03 and 0.35 ± 0.04 at 6, 21 ($p<0.05$) and 32 dpi ($p<0.001$), respectively). However, the values obtained at the end of the experiment were similar between groups.

The rate-dependent depression (RDD) of the H reflex (*Figure 2F*) showed that while control animals had complete depression of their H wave after 10 consecutive stimuli at 5Hz, the SCI animals had less reduction. The area under the curve (*Figure 2H*) obtained from the depression profile of the plantar muscle (*Figure 2G*) showed that the SED, EE and TR groups area was significantly higher compared to control animals (SED 149.02 ± 14.99 ($p<0.01$), EE: 170.82 ± 12.36 ($p<0.001$); TR: 145.04 ± 16.09 ($p<0.05$) vs CTRL: 90.91 ± 6.86), indicating marked reduction of the H wave RDD due to the interruption of descending spinal pathways. In contrast, the WR group showed a slight reduction of the area under the curve at the end of the experiment, with values not significantly difference with respect to control animals (WR: 123.93 ± 18.26).

We further questioned whether the locomotor improvement observed in the WR group was influenced by the reduction of hyperreflexia. To answer that question, we correlated the locomotion scores of animals from the groups with higher MEPs (EE and WR), as this parameter could also influence motor recovery, with their $H_{max}/M_{max}$ ratio at 32 dpi. As shown in *Figure 2I*, there was a strong correlation between the H wave modulation and the BMS score ($R=-0.75$, $p=0.0034$), indicating that a better modulation of the spinal reflexes may be associated with improved locomotion in SCI mice subjected to voluntary wheel running.

**Activity-based therapies contribute to maintain spinal PNN after SCI**

To analyze changes in spinal cord PNN after SCI and the possible modulation by activity-based therapies, we evaluated the intensity of aggrecan labeling (*Figure 3A, 3B*). Aggrecan is a chondroitin-sulfate proteoglycan (CSPG) and the main constituent of PNN (18). In fact, it labels more PNN than the marker Wisteria floribunda agglutinin (WFA) in the spinal cord (15). Aggrecan immunostaining (*Figure 3B*) of the lumbar spinal cord revealed that PNN around motoneurons were significantly reduced 5 weeks after SCI in the injured-SED group (48.2 ± 3.6% of reduction ($p<0.001$) vs intact CTRL). In contrast, we found that WR and TR significantly prevented PNN reduction (WR: 0 ± 4.9% and TR: 22.8 ± 4.3% reduction), whereas the EE group did not (EE: 29.4 ± 6.3% reduction, ($p<0.05$) vs CTRL). Comparatively, PNN preservation was greater in the WR group than the rest of the treated groups (WR vs EE $p<0.05$). This effect seems related to the amount of physical activity since the WR group run

much more than the TR group during the 4 weeks of follow-up ($p<0.001$; *Figure 3C*). In addition, within the WR group, there were also differences in the distance run per day, which positively correlated ($R=0.79$) with PNN preservation.

Next, we assessed the proprioceptive contacts on the lumbar motoneurons using the VGlut1 marker, which is specific for Ia sensory afferents from the muscle spindle (19) (*Figure 3A, 3E*). We found that all activity-treated groups presented increased VGlut1 staining compared to sedentary animals (EE: 1.264± 0.17, WR: 1.29 ± 0.05, TR: 1.27 ± 0.05 vs SED: 0.85 ± 0.04, $p<0.01$ in all groups), but only the WR group presented more VGlut1 staining than control mice (WR vs CTRL: 1 ± 0.03, $p<0.05$).

Lastly, to examine the progression of PNN and VGlut1 preservation over time, a second experiment was conducted with two SCI groups which were followed-up for 11 weeks and one of them was submitted to the treadmill protocol (*Suppl Figure 1B*). At 10 weeks after the injury, no significant differences were observed neither in PNN integrity (CTRL: 1 ± 0.11; SED: 0.77± 0.1, TR: 0.89± 0.13) nor in VGlut1 staining (CTRL: 1 ± 0.08; SED: 0.92 ± 0.07; TR: 1.12 ± 0.16).

**Activity-based therapies modulate the expression of KCC2 after SCI**

In order to assess whether PNN reduction by the SCI could alter the physiological properties of lumbar motoneurons, we evaluated the expression of potassium chloride cotransporter KCC2, which is necessary to maintain the inhibitory GABAergic tone (20). We found that the SCI significantly reduced KCC2 staining in the ventral horn (SED: 0.52± 0.01 vs CTRL: 1± 0.06 ($p<0.001$), *Figure 3F*). We further observed that mice of the TR group, similar to sedentary ones, presented significantly decreased KCC2 immunoreactivity compared to control animals (TR: 0.71± 0.04 vs CTRL; $p<0.05$). On the other hand, the EE and WR groups showed a preserved expression of KCC2 with similar values to control animals, and significantly higher than sedentary animals (EE: 0.86± 0.08 ($p<0.05$) and WR: 1.07± 0.07 ($p<0.0001$) vs SED). Interestingly, linear regression analysis showed a significant correlation between PNN and KCC2 expression ($R= 0.7$, $p<0.0001$, *Figure 3G*).

**Activity-based therapies modify the glial reactivity and nociceptive nonpeptidergic C-fibers after SCI**

To assess the role of activity-dependent therapies in the modulation of the inflammatory response after SCI, we analyzed the expression of two hallmarks of inflammation: GFAP, to label astrocytes and Iba1, a marker of microglia/macrophages (*Figure 4A, 4B, 4C).* As expected, there was a significant increase in astroglial reactivity in the ventral horn (*Figure 4B*) in all injured animals compared to control ones (SED: 1.94 ± 0.28 ($p<0.05$); EE: 2.34 ± 0.3 ($p<0.001$); WR: 2.01 ± 0.127 ($p<0.01$); TR: 2.24 ± 0.27 ($p<0.01$) *vs.* CTRL: 1 ± 0.08), without changes in the groups receiving activity-based strategies. In contrast, we found that levels of Iba1 microglial marker presented a slight but not significant increase in SCI sedentary mice compared to control mice (SED: 1.95 ± 0.28 vs. CTRL: 1 ± 0.10). However,

enriched environment and voluntary wheel treatments induced a significant increase in the expression of Iba1 in the ventral horn (EE: 3.51 ± 0.82 ($p<0.001$), WR: 3.35 ± 0.22 ($p<0.001$) vs CTRL). This marked increase could be attributed to changes in microglial morphology more than an increased in the number of microglia. These changes were not observed in the treadmill group (2.25 ± 0.41).

Next, we wanted to ascertain whether the differences in pain sensitivity were related to changes in glial reactivity in the dorsal horn at L6 (*Figure 4C*). The absence of differences between groups in both immunostainings might indicate that the inflammatory milieu generated by the thoracic injury did not reach level L6. In fact, only the EE group presented a significant increase of astrogliosis compared to the other groups (EE: 1.49 ± 0.07 vs CTRL: 1 ± 0.03 ($p<0.001$), SED: 1.15± 0.09 ($p<0.05$), WR: 1.18± 0.07 ($p<0.05$)). Finally, nociceptive nonpeptidergic C-fibers were labelled by IB4 marker (*Figure 4D*). IB4+ staining was found in the lamina II of the dorsal horn, which was unaffected by the injury (SED 0.906 ± 0.087 vs CTRL 1.052 ± 0.048). In contrast, WR and TR groups presented a significant reduction on IB4+ staining (WR: 0.798 ± 0.055 ($p<0.05$); TR: 0.708 ± 0.014 ($p<0.01$) vs CTRL). However, this reduction was not observed in the EE group (EE: 0.967 ± 0.093).

**PNN in the dorsal column nuclei are differently modulated by activity-dependent therapies than spinal PNN after SCI**

Given the importance of sensory input in regulating PNN, we hypothesized that the dorsal column nuclei, which receives sensory information from the hindlimbs, could present altered PNN integrity after SCI (*Figure 5A*). Considering the gracile nucleus (*Figure 5B*), quantitative analysis of aggrecan staining showed that the SCI did not produce changes in PNN expression (SED: 0.89± 0.06 vs CTRL 1.00 ± 0.07). However, some activity-dependent therapies could modulate PNN since EE (0.45± 0.03) and WR (0.48 ± 0.11) groups showed significantly reduced expression of PNN compared to control ($p<0.0001$) and SED groups ($p<0.01$ vs. EE and $p<0.05$ vs. WR). TR group (0.77 ± 0.10) did not show significant differences either between control or sedentary animals. Regarding the cuneatus nucleus (*Figure 5C*), the injury produced a slight but not significant increase in the aggrecan staining (SED: 1.25 ± 0.14 vs. CTRL 1.00 ± 0.12). Moreover, in this nucleus, all the activity-based therapies reduced the expression of PNN compared to the SED group (EE: 0.65± 0.04 ($p<0.01$), WR: 0.60± 0.07 ($p<0.01$), TR: 0.84±0.08 ($p<0.05$) vs. SED).

## DISCUSSION

During the past decades, intense research has focused on overcoming the inhibitory influence of proteoglycans after SCI, mainly by a general application of chABC. This approach, although very promising, could have masked the specific role of spinal PNN after injury. Here, we wanted to evaluate how a SCI and different types of physical activity could affect PNN around spinal motoneurons caudal to the injury and thus, to further understand the role of these nets in the functionality of spinal circuits. Finally, the fate of PNN in dorsal column nuclei in the brain stem after SCI was also evaluated.

### Effects of SCI and activity-based therapies on lumbar PNN

We found that the contusion on the thoracic spinal cord produced a reduction of lumbar PNN after the injury. The partial disappearance of PNN could be explained by a decreased activity in motoneurons (21) produced not only by the interruption of descending inputs but also by the reduced sensory input from the muscle spindles caused by the paresis of the hindlimb. Indeed, a reduction of aggrecan expression around motoneurons was reported after paralyzing hindlimb muscles with botulinus toxin A (22). Complementary, metalloproteases, the proteolytic enzymes that degrade PNN, become upregulated after SCI which could also contribute to PNN reduction (23).

In contrast to our findings, a previous work pointed out that after a cervical spinal cord hemisection, there is a fast increase of PNN and proteoglycans around phrenic motoneurons (10). However, that study did not quantify the changes in PNN and mainly showed an increased immunoreactivity of proteoglycans in the ventral horn. In contrast, we specifically measured aggrecan intensity in PNN surrounding lumbar motoneurons. Moreover, it is not surprising that the hindlimb paralysis caused by the SCI decreased PNN in the lumbar spinal cord since previous works have already demonstrated that, in contrast to cortical PNN, neural activity increases lumbar spinal PNN (5,6). In our study, the application of the different activity-dependent therapies reverted the decrease of PNN induced by the injury, being the voluntary wheel running the most effective protocol preserving these nets.

To understand the differential effect of the three types of activities is important to note that, in our study, the enriched environment did not favor intense physical activity, as the wheel was blocked, whereas the paper tissue elicited fine-motor activity to build the nest. However, the WR group included both an enriched environment and full access to a wheel during all the follow-up. In contrast, animals submitted to a forced and ruled physical activity were kept in standard cages and physical exercise was limited to 20 minutes per day in a treadmill, with an intensity adapted to the locomotor capabilities of each mice. This fact could explain the weaker effect of the TR group on spinal PNN compared to previous works (6). Altogether, our results suggest that the quantity and intensity of physical activity performed may be crucial in determining the degree of PNN modulation. In fact,

previous work in our laboratory already pointed out that the amount and not the type of physical activity is important for the maintenance of spinal PNN after neural injuries (24).

The potential of physical rehabilitation to favor motor recovery after SCI has been related with increased expression of neurotrophic factors (25,26) and activation of the spinal circuits, which integrate sensory information to generate appropriate motor responses without supraspinal inputs (27). In addition, segmentary sensory inputs are crucial for the maintenance of spinal PNN mediated by physical activity (6). Briefly, during exercise, activation of motoneurons either by segmentary reflexes or spare descending motor tracts could mediate PNN formation through activation of AMPA receptors (AMPAr). In fact, in cortical interneurons, calcium influx via AMPAr and L-type channels is necessary for the activity-dependent formation of PNN (21).

On the other hand, several works have highlighted the potential of enriching activities to modulate cortical (28–30) and cerebellar PNN (4). However, to our knowledge, there are no previous studies analyzing the impact of enriching stimuli on spinal PNN. Regardless of the anatomical location, enriched stimuli produce epigenetic changes in the neuron transcription machinery affecting genes involved in synaptic signaling and plasticity (31,32). These changes in chromatin remodeling are tightly related to PNN since were first described in the visual cortex during the critical period (33). Exposure to an enriched environment, with free access to a wheel, had beneficials effects on the sensorimotor functions of adult mice, with improved equilibrium, motor coordination and muscular strength (34). In a recent study, it enhanced the activity of proprioceptive neurons and increased their regenerative potential in an experimental model of SCI (30). These effects were also mediated by epigenetic reprogramming in proprioceptive neurons. Therefore, similar to cerebellar PNN (4), regulation of spinal PNN could be mediated by a synergistic effect between intrinsic and extrinsic factors.

It is important to note that the improvements of BMS score over time observed in the WR group and slightly shown also in EE talk in favor of a time-dependent progression that may be facilitated by these treatments. However, the effects of activity on PNN observed at 35 dpi were not found in the long-term experiment, in which there were no differences in PNN levels between the studied groups. Probably, the spontaneous recovery and the increased locomotor activity observed after this mild injury, progressively provided the necessary input to increase spinal PNN and consequently neutralized the effect of activity-dependent therapies.

**Effects of activity-based therapies on functional and electrophysiological outcomes after SCI**

SCI does not only lead to loss of motor and sensory function but also facilitates the appearance of spasticity and neuropathic pain, which are related to maladaptive plasticity after the injury. We observed that SCI mice developed hyperreflexia and hyperalgesia. Activity-dependent therapies reduced them, although with variable effects depending on the type of activity applied. Voluntary

wheel running was able to modulate both alterations, whereas treadmill running only attenuated hyperalgesia after SCI. Previous works have already demonstrated that physical exercise can modulate both neuropathic pain and spasticity after SCI (13,14).

The H-wave, typically altered after SCI, was recovered by bike-training in SCI animals, and these changes were related with normalized levels of KCC2 in the lumbar spinal cord (13), similarly to what we described in the WR group. In contrast, our forced exercise protocol had no effects on these parameters, probably due to the lower amount of activity performed compared to the WR group. In fact, we found a relationship between the functionality of spinal circuits and lumbar spinal PNN. Changes in PNN may contribute to the development of hyperreflexia by several mechanisms. First, a reduction of the inhibitory responses of motoneurons has been attributed to changes in the intracellular [Cl-] balance due to a reduction of cation-chloride cotransporters (CCC). However, recent work points out that proteoglycan sulfates found in PNN determine the homeostatic set point of Cl- and hence, neuron polarity of GABA signaling (35). Thus, the reduction of negative extracellular charges may modify the transmembrane Cl- gradient (36), altering the inhibitory synaptic potentials and impairing network excitability (35,37,38). Moreover, the reduction in the KCC2 transporter found in the SCI mice has been linked to the excitatory state of motoneurons and contribute to the development of hyperreflexia (39). Secondly, the mice submitted to wheel running had significant preservation of spinal PNN and, in parallel, showed electrophysiological H-reflex parameters closer to control animals. Besides, our findings give support to the previous suggestion that optimal neuronal excitability provided by PNN preservation together with modulation of stretch reflex by proprioceptive afferent activation may contribute to locomotion recovery (40).

We also found that activity-based therapies significantly increased the density of glutamatergic VGlut1+ terminals around spinal motoneurons, even above control levels. A previous study demonstrated that there is a competition between proprioceptive terminals and corticospinal descending inputs to contact spinal motoneurons (41). Thus, the increased activity of proprioceptive fibers together with a reduced descending input due to the SCI, increases primary afference inputs to motoneurons from injured animals exposed to activity. However, besides the number of contacts, other factors determine the effectiveness of these synapses. In fact, similar to GABA responses, the effectiveness of glutamatergic signaling through AMPAr is also related to this net-like extracellular matrix (42,43). Hence, it is feasible that proprioceptive neurons and PNN present mutual and positive feedback: while proprioceptive activation might participate in the synthesis of PNN components, the presence of PNN potentiates the excitatory synaptic response.

Regarding neuropathic pain, a thoracic SCI produced thermal allodynia which was reversed by therapies that increased physical activity, such as treadmill running or voluntary running in a wheel, but not when animals were just kept in an enriched environment. In the literature, different protocols

of exercise have been able to revert mechanical and sometimes thermal hyperalgesia after diverse SCI models (14,44). In our model, the reduction in neuropathic pain was not related with changes in microglia reaction, since we did not find microgliosis at the L5-L6 segments where nociceptive afferents from the hind paw enter in the spinal cord. A previous study also found that activation of mechanosensory afferents did not induce microglial proliferation in the dorsal horn of the spinal cord (45).

Strikingly, sensorimotor activity induces structural changes in the nociceptive system, as we observed that those animals with reduced pain presented less IB4+ staining. During the painful state, there is a process mediated by IB4+ cells called hyperalgesic priming, that drives the progression of acute pain into a chronic state (46,47). Besides, the reduction of thermal hyperalgesia and decrease of IB4+ staining in the dorsal horn by physical exercise has also been observed in a SCI model of chronic neuropathic pain (44).

Since enriched environment and treadmill groups presented similar levels of PNN but not similar latency withdrawal in the thermal test, it seems clear that PNN do not contribute to neuropathic pain in this model. However, our study focuses on PNN around motoneurons. It would be interesting to study the implications of the fewer PNN located in the dorsal horn (48), as overexpressing Sema3A, the inhibitory-component of PNN, in injured animals prevented pain development (49).

**Differential effects of SCI and activity-based therapies on PNN in spinal cord and brainstem**

A current challenge in the PNN field is to understand why PNN are differently regulated by activity depending on the anatomical localization. In this study, we also evaluated how SCI affected PNN in the dorsal column nuclei, the brainstem centers that process limb sensory information (50). The gracile nucleus is classically considered the sensory relay of fine sensation from the hindlimb, being the cuneate nucleus the equivalent for the forelimb (51). However, recent work points out that while the gracile nucleus only processes the hindlimb fine tactile information, cuneate nucleus integrates the forelimb fine tactile and the fore and hindlimb proprioceptive information (52). Therefore, we analyzed PNN of both nuclei. On the one hand, *Massey et al (2006).* had already shown that a cervical SCI increased PNN in the cuneatus nucleus, although no quantification was presented in the paper (9). Contrarily, we only observed a non-significant increase of PNN. Being the relay of proprioceptive inputs also from the forelimb, our thoracic injury induced only partial denervation of cuneatus' neurons, that could mask the effects of the injury on their PNN. On the other hand, the injury did not affect PNN in the gracile nucleus, relay of tactile inputs from the hindlimb.

Considering the effect of activity on both brain stem nuclei, we could observe a clear reduction of PNN by the enriched environment and voluntary exercise, whereas the treadmill protocol only reduced PNN in the cuneate nucleus. Probably, the maintenance of PNN on these nuclei could be also mediated by

descending inputs from higher somatosensory centers (51) and not just by direct projections from peripheral neurons. In fact, several works have already demonstrated that enriching activities reduces PNN from sensory cortices (34, 36). Therefore, since proprioceptive afferents are key neurons mediating activity-dependent plasticity (30), all type of activities modulated PNN in the cuneate nuclei. In contrast, activation of tactile afferents could be more important in the context of enriched environments.

In conclusion, the present study evidences that SCI has a direct impact on PNN around spinal motoneurons caudal to the injury, and that different types of activity can modulate the expression of PNN, together with beneficial effects on functional outcome after the injury. We propose that these PNN have a relevant influence on motoneuron excitability and synaptic connectivity. The modulation of PNN expression emerges as a versatile target to treat neuronal disorders that either need to boost plasticity or protect synaptic integrity.

## Experimental procedures

### Experimental groups

All experimental procedures were conducted in accordance with the Universitat Autònoma de Barcelona Experimentation Ethical Committee (CEEAH 1188R3-DMAH 6131) and followed the European Communities Council Directive 2010/63/EU. A total of 54 adult female mice (18-25g; 8 weeks, C57BL/6J, Charles River Laboratories) were housed at room temperature of 22± 2 ºC and on a 12h light/dark cycle. Food and water were provided *ab libitum*.

Two sets of experiments were performed in this study for characterizing functional and histological outcomes produced at 5 weeks (Experiment 1) and at 11 weeks (Experiment 2) after the injury (*Figure 1*). The first experiment had five groups of mice. Initially, animals were divided in control (uninjured; *n*=5) or SCI (*n*=23) groups. Seven days after the injury, injured mice were further divided into four different treatment groups, a sedentary group (SED, *n*=5), and three groups submitted to activity-dependent therapies: enriched environment (EE, *n*=6), voluntary wheel (WR, *n*=7) and forced treadmill running (TR, *n*=5). The second experiment had three experimental groups: control (CRTL, *n*=10), SCI + sedentary (SED, *n*=8) and SCI + forced treadmill running (TR, *n*=8). All injured animals were randomly divided into the different experimental groups. In case unbalanced groups were generated, it was corrected using their tissue displacement and their Basso Mouse Scale (BMS) score at 7 dpi (days post-injury).

### Spinal cord injury

Surgical procedures were performed under general anesthesia using an intraperitoneal injection (*i.p.*) of ketamine (90 mg/kg) and xylazine (10 mg/kg) in saline solution. After laminectomy, a moderate spinal cord contusion was performed at T11 using a force-controlled spinal cord impactor (Infinite Horizon Impactor Device). The applied force was set to 50 KDyn, which induced a tissue displacement around 300-490 μm. After surgery, animals received 1mL of saline subcutaneously to prevent dehydration. Postoperative care consisted of subcutaneous injections of buprenorphine (0.1 mg/kg) for three days and manual bladder voiding twice a day until voiding reflex returned.

### Activity-based therapies protocol

Enriched environment (EE)

The enriched environment consisted of social housing (6 animals) in a cage (364 × 258 x 350mm$^3$; Activity Wheel Cage System for mice, Tecniplast, Buguggiate, Italy) equipped with the wheel blocked and with tissue paper added as naturalistic bedding that stimulates fine-motor activity.

Voluntary wheel running (WR)

One week after injury, injured animals were housed in a cage equipped with a free-to-access running wheel (364 × 258 × 350mm$^3$; Activity Wheel Cage System for mice, Tecniplast, Buguggiate, Italy). The wheels were connected to a wheel revolution count to daily calculate the running distance using the diameter of the wheel (21 cm). In order to avoid animal isolation, animals were housed in pairs, a group size that also ensured that both animals could run at the same time.

Forced treadmill running (TR)

Four days before the surgical procedure, all mice were familiarized with the treadmill (Treadmill LE 8706). The habituation protocol consisted of running for 15 min at a speed of 11 cm/s. The standard negative stimulus (a 0.1 mA low electric shock) was used. Mice started the treadmill training one week after SCI and were exercised 5 days/week for 4 weeks (Experiment 1) or 10 weeks (Experiment 2). After surgery, the negative stimulus was replaced by a gentle tapping of the tail to encourage running when mice stopped. The training protocol consisted of running for 5 min at a speed of 11-14 cm/s and 15 min at an increasing velocity adapted to mice recovery. At the last training sessions, animals reached a maximum velocity of 24 cm/s.

**Functional assessment**

Basso Mouse Scale

Motor recovery was assessed in an open field using the BMS at 3, 7, 14, 21, 28 and 35 days after the injury. BMS is a nine-point scale that ranges from 0 to 9, which 0 means total paralysis and 9 reflects normal locomotion. The analysis was performed by two researchers which followed blinding procedures to establish the score of each animal. The score of each animal was the average score of each hind paw.

Algesimetry tests

Neuropathic pain was evaluated carrying out thermal algesimetry test, using a Plantar algesimeter device (Ugo Basile). Some days before the preoperative testing and the surgery, animals were acclimated to the testing chamber for three days (15 minutes/day). Then, tests were performed preoperatively to establish baseline values, at 14 and 28 days after the injury by a blinded researcher. A light beam (intensity=30) was applied to the hind paw until the animal withdrew the paw (53). The paw withdrawal latency was recorded three times, with a resting time between trials, and averaged. Finally, values were normalized to those of control intact animals. To categorize animals with hyperalgesia, we first calculated the intra-group variability of control animals during the whole experiment. Then, those injured animals that presented a higher mean ± control variability compared to their basal value were categorized as animals with hyperalgesia.

Electrophysiological tests

Electrophysiological test were performed before SCI (basal values) and at 6, 21 and 32 days after injury with the animals under anesthesia (ketamine 90 mg/kg and xylazine 10 mg/kg), since it has negligible effects on the electrophysiological recording (54). During the tests, a heating pad was used to maintain body temperature and a microscope was used to ensure reproducibility of needle location on all animals.

Spasticity was analyzed by measuring the H wave and its RDD in the plantar muscle, assuming that the changes observed in that muscle are characteristic for the hindlimb musculature (55). Firstly, we evaluated the maximum amplitudes of the M wave ($M_{max}$; direct muscle response) and the H wave ($H_{max}$; monosynaptic reflex) of the plantar interosseus muscle. Then, we calculated the ratio $H_{max}/M_{max}$ (56), as an index of the excitability of the Ia afferent synapse on spinal motoneurons. To assess the effect of activity in modulating hyperreflexia, only injured animals that presented hyperreflexia after the injury (6 dpi $H_{max}/M_{max}$ ratio > basal $H_{max}/M_{max}$ ratio) were included in the study. Then, we measured the changes in the H wave amplitude over consecutive stimulations, known as the rate-dependent depression (RDD) whose alteration is a hallmark of spastic animals (56). For both measurements, we initially delivered single electrical pulses of 0.02 ms (Grass S88) by a needle inserted percutaneously at the sciatic notch. The recorded potentials were amplified and displayed on a digital oscilloscope (Tektronix 450S). While $M_{max}$ was obtained with supramaximal stimulation, the $H_{max}$ was elicited after trying a range of increasing stimulus intensities. The stimulation intensity that gave the $H_{max}$ was then used for the RDD test. The RDD was measured performing trains of ten consecutive pulses at different frequencies (1, 5 and 10 Hz) with at least 30 seconds rest between each train. RDD values were expressed as the percentage of the ratio between the last ($10^{th}$) and the first pulse. Then, in each experimental time-point, a curve expressing the % RDD (y-axis) at different frequencies (x-axis) was generated to further calculate the area under the curve for each animal.

Finally, we recorded the MEP of the plantar interosseus, tibialis anterior and gastrocnemius muscles to evaluate descending pathways (57). MEP values were presented as the percentage (%) of recovery using the basal value of each animal. Stimulation was delivered by means of needle electrodes subcutaneously placed overlaying the sensorimotor cortex and applying pulses of 0.1 ms duration and supramaximal intensity.

**Histological evaluation**

Five (Experiment 1) or eleven (Experiment 2) weeks after the SCI, mice were euthanized with pentobarbital (*i.p.*; 200 mg/kg). Animals were transcardially perfused with cold 4% paraformaldehyde in 0.1M phosphate buffer (PB). Then, brains and spinal cords were dissected out and post-fixed in 4% paraformaldehyde in PB overnight and 2h, respectively. Tissues were cryoprotected in 30% sucrose solution in PB at 4ºC until they sank.

For the spinal cord, the lesion site (T11) and the lumbar region (L4-L6) were serially cut on a cryostat (15 μm thick transverse sections) and collected onto gelatin-coated glass slides. Thoracic sections were used to evaluate demyelination with Luxol Fast Blue staining (LFB; Sigma-Aldrich) (58). Briefly, after a dehydration phase, slides were placed in a 1mg/mL LFB solution in 95% ethanol and 0.05% acetic acid at 37ºC overnight. Then, sections were washed in 95% ethanol and distilled water before being placed into a 0.05% $Li_2CO_3$ solution for 2:30 minutes at room temperature (RT). After another dehydration, sections were mounted in DPX mounting medium (Sigma-Aldrich).

A subset of cord sections was used to recognize the L5 and L6 segments after incubation in a cresyl-violet acetate solution for 3h at RT. L5 sections were used to analyzed PNN, VGlut1 staining, the potassium chloride cotransporter KCC2 and glial reactivity (GFAP and Iba1), while L6 sections were used for glial reactivity and IB4 afferences (*Figure 1*). For glial reactivity, PNN and VGlut1 staining, slides were blocked with 10% normal donkey serum (NDS) for 1h. For KCC2, sections were permeabilized with PBST-BSA 3% during 45 minutes at RT and then, nonspecific interactions were blocked with PBS-BSA 3% and 10% normal donkey serum for 1h at RT. In all cases, sections were then incubated overnight at 4ºC with the primary antibody (Table 1). After washes, immunoreactive sites were revealed using species-specific secondary antibodies (Table 1). After 2h of incubation at RT, FluoroNissl Green (1:200) was added diluted in PBS in some immunohistochemical labeling. Sections were mounted in Fluoromount-G medium (Southern Biotech).

To analyze changes in the dorsal column nuclei, 3 mm of brainstem were serially cut on the cryostat (20 μm thick transverse sections). Then, PNN were immunostained using Aggrecan and the VGlut1 staining was used to identify the cuneatus nucleus (52). Only those sections containing the nuclei (Bregma -7.64 to -8.24) were quantified.

**Histological analysis**

Myelin sparing was calculated by delineating the spared LFB-stained tissue area as well as the whole spinal cord area from images taken at the epicenter of the injury and every 150 μm rostral and caudal to the lesion. Both areas were used to calculate the % of spared white matter.

For lumbar sections, grayscale microphotographs were captured at 40x in the ventral horn (L5) and at 20x in the dorsal horn (L6). The background was corrected, and the threshold was defined for all the microphotographs of the same marker. For glial reactivity quantification, integrated density of immunoreactivity was measured in the full image of the ventral horn, and in a region of interest (ROI) of 230 $\mu m^2$ of the dorsal horn. IB4+ area in laminae I-II was traced to quantify the intensity of labeling. KCC2 immunoreactivity was quantified measuring the integrated density of a band of 2 μm around FluoroNissl Green positive neurons in the ventral horn. At least five sections per marker from each

animal were used to calculate the mean value. In the KCC2 analysis, a minimum of 25 neurons was measured for each animal. Immunolabeled images were acquired with a digital camera Nikon DS-Ri2 attached to a Nikon Eclipse Ni-E microscope. Image analysis was performed by Fiji software.

To measure PNN expression and VGlut1 positive fibers on lumbar motoneurons, images were taken from four or five cord sections under a confocal laser-scanning microscope (Z stack image of step 0.5; Leica TCS SP5) at 40x. To quantify PNN changes, a minimum of 30 motoneurons (identified by FluoroNissl Blue labeling, located within the ventral horn and presenting an area >350$\mu m^2$ (59) (*Suppl Figure 1A*)) were measured for each animal. After background correction, the maximal projection of the different z-stacks was done and then, a band of 4 μm around PNN was calculated to measure the integrated density of that region. For measurements of VGlut1-positive fibers, the VGlut1-positive boutons present in a band of 4 μm around the selected motoneurons were counted. PNN thickness in the dorsal column nuclei were determined using the same method used to measure spinal PNN.

**Statistical analysis**

Data is reported as mean ± standard error of the mean (SEM). Normality was assessed by Shapiro-Wilk test that showed that all quantitative data followed a normal distribution. Thus, the functional and electrophysiological results including motor and sensory tests were analyzed by two-way repeated-measures ANOVA with group and time after injury as factors, followed by Bonferroni *post-hoc* tests. Histological results were analyzed by one-way ANOVA with Bonferroni *post-hoc* test, except for Luxol fast blue analysis in which we used a two-way ANOVA (group × distance in the spinal cord). Pearson's correlation and linear regression analysis were used to correlate H-reflex modulation with BMS score and the PNN thickness with the distance run/day in the WR group. Statistical analysis was done using GraphPad Prism 7 software. A p-value $<0.05$ was used to indicate significant differences between groups.

## Acknowledgments

This work was funded by the Fundació La Marató-TV3 (TV3-201736-30-31).

The authors research was supported by funds from CIBERNED and TERCEL networks, co-funded by European Union (ERDF/ESF, "Investing in your future"). JSV holds a predoctoral fellowship of the AGAUR, Secretaria d'Universitats i Recerca del Departament d'Empresa i Coneixement de la Generalitat de Catalunya, cofunded by European Social Funds.

The authors appreciate the technical help of Mònica Espejo, Jessica Jaramillo and Neus Hernández, the aid of Dr. Jesus Amo during the BMS test, and the critical revision and contributions of Dr. Xavier Navarro (Universitat Autònoma de Barcelona).

## Authors contributions

JSV contributed to the design of the experiments, performed the experiments, analyzed the data and wrote the original draft of the manuscript. LJ contribute to the design of the experiments and reviewed and edited the manuscript. CP performed some of the experiments and reviewed and edited the manuscript. EU acquired the funding, designed the study and experiments, performed some of the experiments, and reviewed and edited the manuscript.

## Declaration of Competing Interest

The authors declare no competing interests.

## REFERENCES


1. Carulli D, Pizzorusso T, Kwok JCF, Putignano E, Poli A, Forostyak S, et al. Animals lacking link protein have attenuated perineuronal nets and persistent plasticity. Brain. 2010;133(8):2331–47.
2. Wang D, Fawcett J. The perineuronal net and the control of cns plasticity. Cell Tissue Res. 2012;349(1):147–60.
3. Pizzorusso T. Reactivation of Ocular Dominance Plasticity in the Adult Visual Cortex. Science (80- ). 2002;298(5596):1248–51.
4. Foscarin S, Ponchione D, Pajaj E, Leto K, Gawlak M, Wilczynski GM, et al. Experience-dependent plasticity and modulation of growth regulatory molecules at central synapses. PLoS One. 2011;6(1).
5. Smith CC, Mauricio R, Nobre L, Marsh B, Wüst RCI, Rossiter HB, et al. Differential regulation of perineuronal nets in the brain and spinal cord with exercise training. Brain Res Bull. 2015;111:20–6.
6. Arbat-Plana A, Torres-Espín A, Navarro X, Udina E. Activity dependent therapies modulate the spinal changes that motoneurons suffer after a peripheral nerve injury. Exp Neurol. 2015;263:293–305.
7. Silver J, Miller JH. Regeneration beyond the glial scar. Nat Rev Neurosci. 2004;(5):146–56.
8. Bradbury EJ, Moon LDF, Popat RJ, King VR, Bennett GS, Patel PN, et al. Chondroitinase ABC promotes functional recovery after spinal cord injury. Nature. 2002;416.
9. Massey JM, Hubscher CH, Wagoner MR, Decker JA, Amps J, Silver J, et al. Chondroitinase ABC Digestion of the Perineuronal Net Promotes Functional Collateral Sprouting in the Cuneate Nucleus after Cervical Spinal Cord Injury. J Neurosci. 2006;26(16):4406–14.
10. Alilain WJ, Horn KP, Hu H, Dick TE, Silver J. Functional regeneration of respiratory pathways after spinal cord injury. Nature. 2011;475(7355):196–200.
11. Wang D, Ichiyama RM, Zhao R, Andrews MR, Fawcett JW. Chondroitinase Combined with Rehabilitation Promotes Recovery of Forelimb Function in Rats with Chronic Spinal Cord Injury. J Neurosci. 2011;31(25):9332–44.
12. García-Alías G, Barkhuysen S, Buckle M, Fawcett JW. Chondroitinase ABC treatment opens a window of opportunity for task-specific rehabilitation. Nat Neurosci. 2009;12(9):1145–52.
13. Cote M-P, Gandhi S, Zambrotta M, Houle JD. Exercise Modulates Chloride Homeostasis after Spinal Cord Injury. J Neurosci. 2014;34(27):8976–87.
14. Detloff MR, Smith EJ, Quiros Molina D, Ganzer PD, Houlé JD. Acute exercise prevents the development of neuropathic pain and the sprouting of non-peptidergic (GDNF- and artemin-responsive) c-fibers after spinal cord injury. Exp Neurol. 2014;255:38–48.

15. Irvine SF, Kwok JCF. Perineuronal nets in spinal motoneurones: Chondroitin sulphate proteoglycan around alpha motoneurones. Int J Mol Sci. 2018;19(4).
16. Sorg BA, Berretta S, Blacktop JM, Fawcett JW, Kitagawa H, Kwok JCF, et al. Casting a wide net: Role of perineuronal nets in neural plasticity. J Neurosci. 2016;36(45):11459–68.
17. Fawcett JW, Oohashi T, Pizzorusso T. The roles of perineuronal nets and the perinodal extracellular matrix in neuronal function. Nat Rev Neurosci. 2019;20(8):451–65.
18. Rowlands D, Lensjø KK, Dinh T, Yang S, Andrews MR, Hafting T, et al. Aggrecan directs extracellular matrix-mediated neuronal plasticity. J Neurosci. 2018;38(47):10102–13.
19. Todd AJ, Hughes DI, Polgár E, Nagy GG, Mackie M, Ottersen OP, et al. The expression of vesicular glutamate transporters VGLUT1 and VGLUT2 in neurochemically defined axonal populations in the rat spinal cord with emphasis on the dorsal horn. Eur J Neurosci. 2003;17(1):13–27.
20. D'Amico JM, Condliffe EG, Martins KJB, Bennett DJ, Gorassini MA. Recovery of neuronal and network excitability after spinal cord injury and implications for spasticity. Front Integr Neurosci. 2014;8:1–24.
21. Dityatev A, Brückner G, Dityateva G, Grosche J, Kleene R SM. Activity-dependent formation and functions of chondroitin sulfate-rich extracellular matrix of perineuronal nets. 2007;n/a-n/a.
22. Kalb R, HockField S. Electrical Activity in the Neuromuscular Unit Can Influence the Molecular Development of Motor Neurons. 1994. p. 539–48.
23. Zhang H, Chang M, Hansen CN, Basso DM, Noble-Haeusslein LJ. Role of Matrix Metalloproteinases and Therapeutic Benefits of Their Inhibition in Spinal Cord Injury. Neurotherapeutics. 2011;8(2):206–20.
24. Arbat-Plana A, Navarro X, Udina E. Effects of forced, passive and voluntary exercise on spinal motoneurons changes after peripheral nerve injury. Eur J Neurosci. 2017;46(12):2885–92.
25. Vaynman S, Ying Z, Gomez-Pinilla F. Interplay between brain-derived neurotrophic factor and signal transduction modulators in the regulation of the effects of exercise on synaptic-plasticity. Neuroscience. 2003;122(3):647–57.
26. Hutchinson KJ, Gómez-Pinilla F, Crowe MJ, Ying Z, Basso DM. Three exercise paradigms differentially improve sensory recovery after spinal cord contusion in rats. Brain. 2004;127(6):1403–14.
27. De Leon RD, Hodgson JA, Roy RR, Edgerton VR. Locomotor capacity attributable to step training versus spontaneous recovery after spinalization in adult cats. J Neurophysiol. 1998;79(3):1329–40.
28. Sale A, Maya Vetencourt JF, Medini P, Cenni MC, Baroncelli L, De Pasquale R, et al.

Environmental enrichment in adulthood promotes amblyopia recovery through a reduction of intracortical inhibition. Nat Neurosci. 2007;10(6):679–81.

29. O'Connor AM, Burton TJ, Mansuri H, Hand GR, Leamey CA, Sawatari A. Environmental Enrichment From Birth Impacts Parvalbumin Expressing Cells and Wisteria Floribunda Agglutinin Labelled Peri-Neuronal Nets Within the Developing Murine Striatum. Front Neuroanat. 2019;13(October):1–14.
30. Madinier A, Quattromani MJ, Sjölund C, Ruscher K, Wieloch T. Enriched housing enhances recovery of limb placement ability and reduces aggrecan-containing perineuronal nets in the rat somatosensory cortex after experimental stroke. PLoS One. 2014;9(3).
31. Rampon C, Jiang CH, Dong H, Tang YP, Lockhart DJ, Schultz PG, et al. Effects of environmental enrichment on gene expression in the brain. Proc Natl Acad Sci U S A. 2000;97(23):12880–4.
32. Fischer A, Sananbenesi F, Wang X, Dobbin M, Tsai LH. Recovery of learning and memory is associated with chromatin remodelling. Nature. 2007;447(7141):178–82.
33. Putignano E, Lonetti G, Cancedda L, Ratto G, Costa M, Maffei L, et al. Developmental Downregulation of Histone Posttranslational Modifications Regulates Visual Cortical Plasticity. Neuron. 2007;54(1):177.
34. García-Mesa Y, López-Ramos JC, Giménez-Llort L, Revilla S, Guerra R, Gruart A, et al. Physical Exercise Protects Against Alzheimer's Disease in 3xTg-AD Mice. J Alzheimer's Dis. 2011;24:421–54.
35. Glykys J, Dzhala V, Egawa K, Balena T, Saponjian Y, Kuchibhotla K V., et al. Local impermeant anions establish the neuronal chloride concentration. Science (80- ). 2014;343(6171):670–5.
36. De Luca C, Papa M. Looking Inside the Matrix: Perineuronal Nets in Plasticity, Maladaptive Plasticity and Neurological Disorders. Neurochem Res. 2016;41(7):1507–15.
37. Miao QL, Ye Q, Zhang XH. Perineuronal net, CSPG receptor and their regulation of neural plasticity. Acta Physiol Sin. 2014;66(4):387–97.
38. Tewari BP, Chaunsali L, Campbell SL, Patel DC, Goode AE, Sontheimer H. Perineuronal nets decrease membrane capacitance of peritumoral fast spiking interneurons in a model of epilepsy. Nat Commun. 2018;9(1).
39. Boulenguez P, Liabeuf S, Bos R, Bras H, Jean-Xavier C, Brocard C, et al. Down-regulation of the potassium-chloride cotransporter KCC2 contributes to spasticity after spinal cord injury. Nat Med. 2010;16(3):302–7.
40. Takeoka A, Vollenweider I, Courtine G, Arber S. Muscle spindle feedback directs locomotor recovery and circuit reorganization after spinal cord injury. Cell. 2014;159(7):1626–39.
41. Jiang YQ, Zaaimi B, Martin JH. Competition with primary sensory afferents drives remodeling of corticospinal axons in mature spinal motor circuits. J Neurosci. 2016;36(1):193–203.

42. Frischknecht R, Heine M, Perrais D, Seidenbecher CI, Choquet D, Gundelfinger ED. Brain extracellular matrix affects AMPA receptor lateral mobility and short-term synaptic plasticity. Nat Neurosci. 2009;12(7):897–904.
43. Sylantyev S, Savtchenko LP, Niu YP, Ivanov AI, Jensen TP, Kullmann DM, et al. Electric fields due to synaptic currents sharpen excitatory transmission. Science (80- ). 2008;319(5871):1845–9.
44. Sliwinski C, Nees TA, Puttagunta R, Weidner N, Blesch A. Sensorimotor activity partially ameliorates pain and reduces nociceptive fiber density in the chronically injured spinal cord. J Neurotrauma. 2018;neu.2017.5431.
45. Hathway GJ, Vega-Avelaira D, Moss A, Ingram R, Fitzgerald M. Brief, low frequency stimulation of rat peripheral C-fibres evokes prolonged microglial-induced central sensitization in adults but not in neonates. Pain. 2009 Jul;144(1–2):110–8.
46. Joseph EK, Levine JD. Hyperalgesic priming is restricted to IB4-positive nociceptors. Neuroscience. 2010;169(1):431–5.
47. Alvarez P, Gear RW, Green PG, Levine JD. IB4-saporin attenuates acute and eliminates chronic muscle pain in the rat. Exp Neurol. 2012;233(2):859–65.
48. Galtrey CM, Kwok JCF, Carulli D, Rhodes KE, Fawcett JW. Distribution and synthesis of extracellular matrix proteoglycans, hyaluronan, link proteins and tenascin-R in the rat spinal cord. Eur J Neurosci. 2008;27(6):1373–90.
49. Tang XQ, Tanelian DL, Smith GM. Semaphorin3A Inhibits Nerve Growth Factor-Induced Sprouting of Nociceptive Afferents in Adult Rat Spinal Cord. J Neurosci. 2004;24(4):819–27.
50. Gordon G, Grant G. Dorsolateral spinal afferents to some medullary sensory nuclei. An anatomical study in the cat. Exp brain Res. 1982;46(1):12–23.
51. Watson C. Chapter 21 - The Somatosensory System. In: Watson C, Paxinos G, Puelles LBT-TMNS, editors. San Diego: Academic Press; 2012. p. 563–70.
52. Niu J, Ding L, Li JJ, Kim H, Liu J, Li H, et al. Modality-based organization of ascending somatosensory axons in the direct dorsal column pathway. J Neurosci. 2013;33(45):17691–709.
53. Hargreaves K, Dubner R, Brown F, Flores C JJ. A new and sensitive method for measuring thermal nociception in cutaneous hyperalgesia. Pain. 1988;32:77–88.
54. Ho SM, Waite PME. Effects of different anesthetics on the paired-pulse depression of the H reflex in adult rat. Exp Neurol. 2002;177(2):494–502.
55. Valero-Cabré A, Forés J, Navarro X. Reorganization of reflex responses mediated by different afferent sensory fibers after spinal cord transection. J Neurophysiol. 2004;91(6):2838–48.
56. Thompson FJ, Reier PJ, Lucas CC, Parmer R. Altered patterns of reflex excitability subsequent

to contusion injury of the rat spinal cord. J Neurophysiol. 1992 Nov;68(5):1473–86.

57. Redondo-Castro E, Navarro X, García-Alías G. Longitudinal evaluation of residual cortical and subcortical motor evoked potentials in spinal cord injured rats. J Neurotrauma. 2016;33(10):907–16.

58. Sánchez-Ventura J, Amo-Aparicio J, Navarro X, Penas C. BET protein inhibition regulates cytokine production and promotes neuroprotection after spinal cord injury. J Neuroinflammation. 2019;16(1):1–12.

59. Friese A, Kaltschmidt JA, Ladle DR, Sigrist M, Jessell TM, Arbera S. Gamma and alpha motor neurons distinguished by expression of transcription factor Err3. Proc Natl Acad Sci U S A. 2009;106(32):13588–93.

## FIGURE LEGENDS

**Figure 1. Schematic representation of the experimental procedure.** (A) Diagram showing the timeline of the experiments. (B) Histological analysis from Experiment 1 at the spinal cord (L5 and L6) and the dorsal column nuclei. PNN: perineuronal net. Individual images were obtained from Biorender and Servier Medical Art.

**Figure 2. Functional evaluation after SCI and activity-based therapies**. (A) Open field locomotion assessed by BMS scale. (B) Neuropathic pain assessment by thermal algesimetry test recorded every two weeks. (C) Averaged percentage of the animals that presented hyperalgesia at the end of the experiment. (D) Representative recordings displaying MEPs in plantar, tibialis anterior and gastrocnemius muscles during the experimental procedure. (E) Quantification of $H_{max}/M_{max}$ changes before initiating the activity-based therapies (6dpi), at 21 dpi and at the end of the experiment (32 dpi). Representative electromyograms showing an initial M wave, resulting from the direct activation of motor axons, and a small wave with longer latency, the H wave, resulting from the monosynaptic activation of lumbar motoneurons by Ia afferences at 6 and 32 dpi. (F) Paired-pulse depression profile of H wave after 10 consecutive stimulations at 1, 5 and 10 Hz. Increasing the frequency of stimulation leads to a dramatic decrease in the H wave amplitude in intact mice compared to injured ones. (G) Depression profile of the H wave at 32 dpi. Statistical differences are not shown. (H) Representation of the area under the curve of the recorded curve of each animal from figure 2G. (I) Relationship between BMS score and H wave recordings in the plantar muscle. *p<0.05, **p<0.01, ***p<0.001 vs control; ##p<0.01, ###p<0.001 vs SED; %p<0.05, %%p<0.01 vs WR, and $p<0.05, $$p<0.01, $$$p<0.001 vs TR; as calculated by two-way ANOVA followed by Bonferroni correction for the multiple comparison. MEP: motor evoked potentials, RDD: rate-dependent depression, BMS: Basso Mouse Scale, CTRL: control, SED: sedentary, EE: enriched environment, WR: voluntary wheel, TR: forced treadmill.

**Figure 3. Histological changes in the lumbar spinal cord after SCI and activity-based therapies.** (A) Representative images of lumbar ventral horn of different histological parameters after SCI and activity-dependent activities. (B) Quantification of PNN labelled with aggrecan (green) around lumbar motoneurons, labelled with FluoroNissl (blue). (C) Average distance run per week over the training period (4 weeks) of the WR and TR groups. (D) Relationship between PNN intensity and distance run per day in the WR group. (E) Quantification of proprioceptive fibers, labelled with VGlut1 (red) in 4µm around lumbar motoneurons, labelled with FluoroNissl (blue). (F) Quantification of the potassium-chloride cotransporter KCC2 (red) around lumbar motoneurons. (G) Relationship between KCC2 and PNN expression in the lumbar spinal motoneurons. *p<0.05, ***p<0.001 vs control; ##p<0.01,

###p<0.001 vs SED; and $p<0.05, $$p<0.01, $$$p<0.001 vs WR; as calculated by one-way ANOVA with Bonferroni multiple comparison. Data are expressed as mean ± SEM normalized to control group. Scale bar: 100 µm (PNN), 50 µm (VGlut1 and KCC2). CTRL: control, SED: sedentary, EE: enriched environment, WR: voluntary wheel, TR: forced treadmill.

**Figure 4. Inflammation and neuropathic pain assessment after SCI and activity-dependent therapies.** (A) Representative images of lumbar L5 ventral and L6 dorsal horn of different histological markers after SCI and activity-based therapies. (B) Quantification of astrocytes and microglia labelled with GFAP (green) and Iba1 (red) at the ventral horn of L5 spinal cord. (C) Quantification of the intensity of glial markers labelled with GFAP (green) and Iba1 (red) at the dorsal horn of L6 spinal cord. (D) Quantification of IB4+ afferences in the dorsal horn of L6 spinal cord. *p<0.05, **p<0.01, ***p<0.001 vs control; #p<0.05 vs SED; $p<0.05 vs WR; as calculated by two-way ANOVA followed by Bonferroni correction for multiple comparisons. Data are expressed as mean ± SEM normalized to control group. Scale bar: 100 µm. CTRL: control, SED: sedentary, EE: enriched environment, WR: voluntary wheel, TR: forced treadmill.

**Figure 5. Modulation of PNN in the dorsal column nuclei after SCI and activity-dependent therapies**. (A) Confocal images of PNN labelled with aggrecan (red in the gracile nucleus and green in the cuneatus nucleus) at 35 dpi. Quantitative analysis of PNN in the gracile (B) and cuneatus nuclei (C) in all groups. Quantitative analysis of ***p<0.001 vs control; #p<0.05, ## p<0.01 vs SED, as calculated by one-way ANOVA with Bonferroni multiple comparison. Data are expressed as mean ± SEM normalized to control group. Scale bar: Scale bar: 50 µm. CTRL: control, SED: sedentary, EE: enriched environment, WR: voluntary wheel running, TR: forced treadmill running.

**Supplemental Figure 1. Lumbar PNN and VGlut1 modulation 11 weeks after SCI.** (A) Representative distribution of motoneurons selected to quantify PNN. (B) Confocal images of PNN, labelled with aggrecan (green) and proprioceptive contacts, labelled by VGlut1 (red) around lumbar motoneurons, labelled with Nissl (yellow) in the lumbar spinal cord at 77 dpi, preceded by the quantitative analyses of aggrecan and VGtlu1 immunostaining. No significant differences were found by one-way ANOVA with Bonferroni multiple comparison. Data are expressed as mean ± SEM normalized to control group. Abbreviations: CTRL: control, SED: sedentary, TR: forced treadmill running.

**Supplemental Figure 2. Tissue damage evaluation after SCI and activity-based therapies.** (A) Quantification of white matter sparing from the injury epicentre to 600 µm rostral and caudal. Total white matter sparing in 1.2mm spinal cord samples of different mice groups. (B) Representative

micrographs showing white matter sparing at the epicentre of the injury in sections stained against LFB from all experimental groups. No significant differences were found as calculated by two-way (myelin sparing) and one-way (total area) ANOVA with Bonferroni multiple comparison. SED: sedentary, EE: enriched environment, WR: voluntary wheel running, TR: forced treadmill running.

TABLE 1. List of antibodies used in the histological analysis

| **Primary antibodies** | | | | **Secondary antibodies** | | | |
|---|---|---|---|---|---|---|---|
| *Name* | *Dilution* | *Host* | *Reference* | *Name* | *Dilution* | *Host* | *Reference* |
| GFAP | 1:1000 | Rabbit | AB5804-Millipore | Alexa 488 | 1:200 | Donkey x Rabbit | A21206-Invitrogen |
| Iba1 | 1:400 | Goat | AB5076-Abcam | Alexa 594 | 1:200 | Donkey x Goat | A11058-Invitrogen |
| Aggrecan | 1:250 | Rabbit | AB1031-Millipore | Alexa 488 | 1:200 | Donkey x Rabbit | A21206-Invitrogen |
| VGlut1 | 1:300 | Guinea Pig | AB5905-Millipore | Cys3 | 1:200 | Donkey x Guinea Pig | 706-165-148-Jackson |
| KCC2 | 1:400 | Rabbit | 07-432-Millipore | Alexa 594 | 1:200 | Donkey x Rabbit | A21207-Invitrogen |
| GSL-I*; Anti-GSL-I | 10 µg/ml 1:500 | - Goat | L-1104-Vector AS2104-Vector | Alexa 488 | 1:200 | Donkey x Goat | A 11055-Invitrogen |

*Lectin from Wisteria Floribunda

# Figure 1

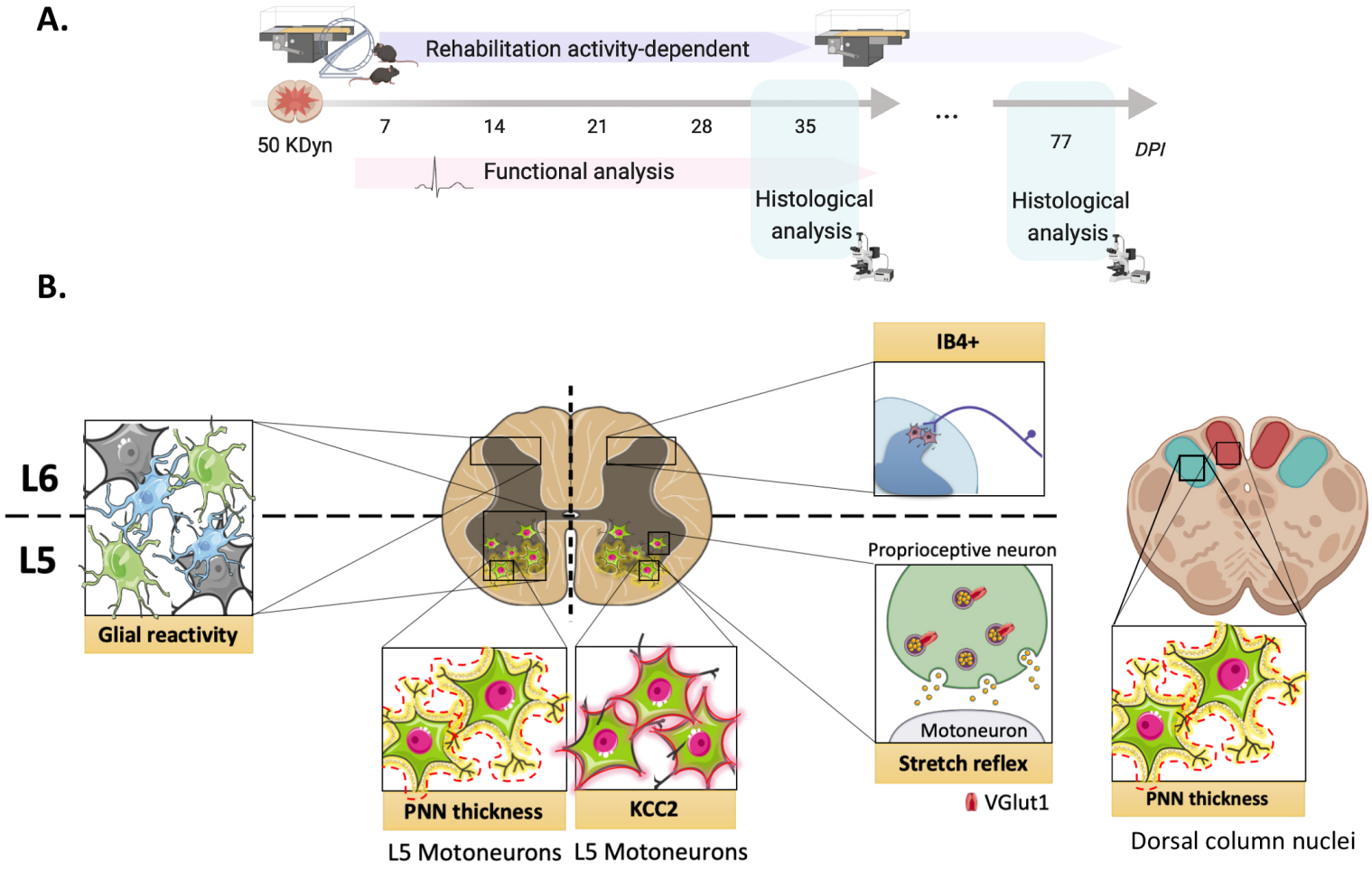
A.
Rehabilitation activity-dependent
50 KDyn
7
14
21
28
35
...
77
DPI
Functional analysis
Histological analysis
Histological analysis
B.
L6
L5
Glial reactivity
IB4+
Proprioceptive neuron
Motoneuron
Stretch reflex
VGlut1
PNN thickness
KCC2
L5 Motoneurons
L5 Motoneurons
PNN thickness
Dorsal column nuclei

# Figure 2

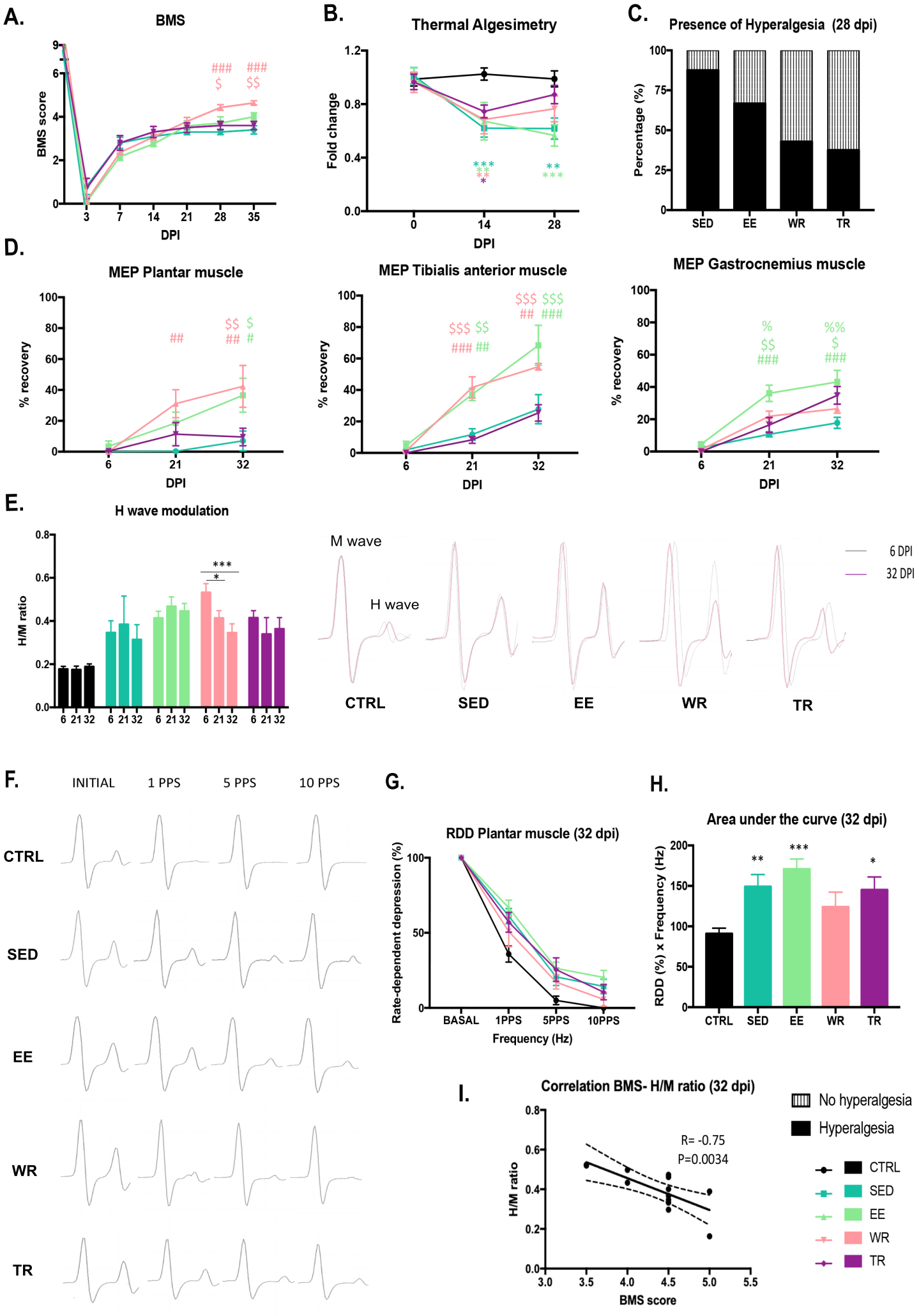
A.
BMS
BMS score
DPI
B.
Thermal Algesimetry
Fold change
DPI
C.
Presence of Hyperalgesia (28 dpi)
Percentage (%)
SED
EE
WR
TR
D.
MEP Plantar muscle
% recovery
DPI
MEP Tibialis anterior muscle
MEP Gastrocnemius muscle
E.
H wave modulation
H/M ratio
M wave
H wave
6 DPI
32 DPI
CTRL
SED
EE
WR
TR
F.
INITIAL
1 PPS
5 PPS
10 PPS
G.
RDD Plantar muscle (32 dpi)
Rate-dependent depression (%)
BASAL
1PPS
5PPS
10PPS
Frequency (Hz)
H.
Area under the curve (32 dpi)
RDD (%) x Frequency (Hz)
I.
Correlation BMS- H/M ratio (32 dpi)
R= -0.75
P=0.0034
BMS score
No hyperalgesia
Hyperalgesia

Figure 3

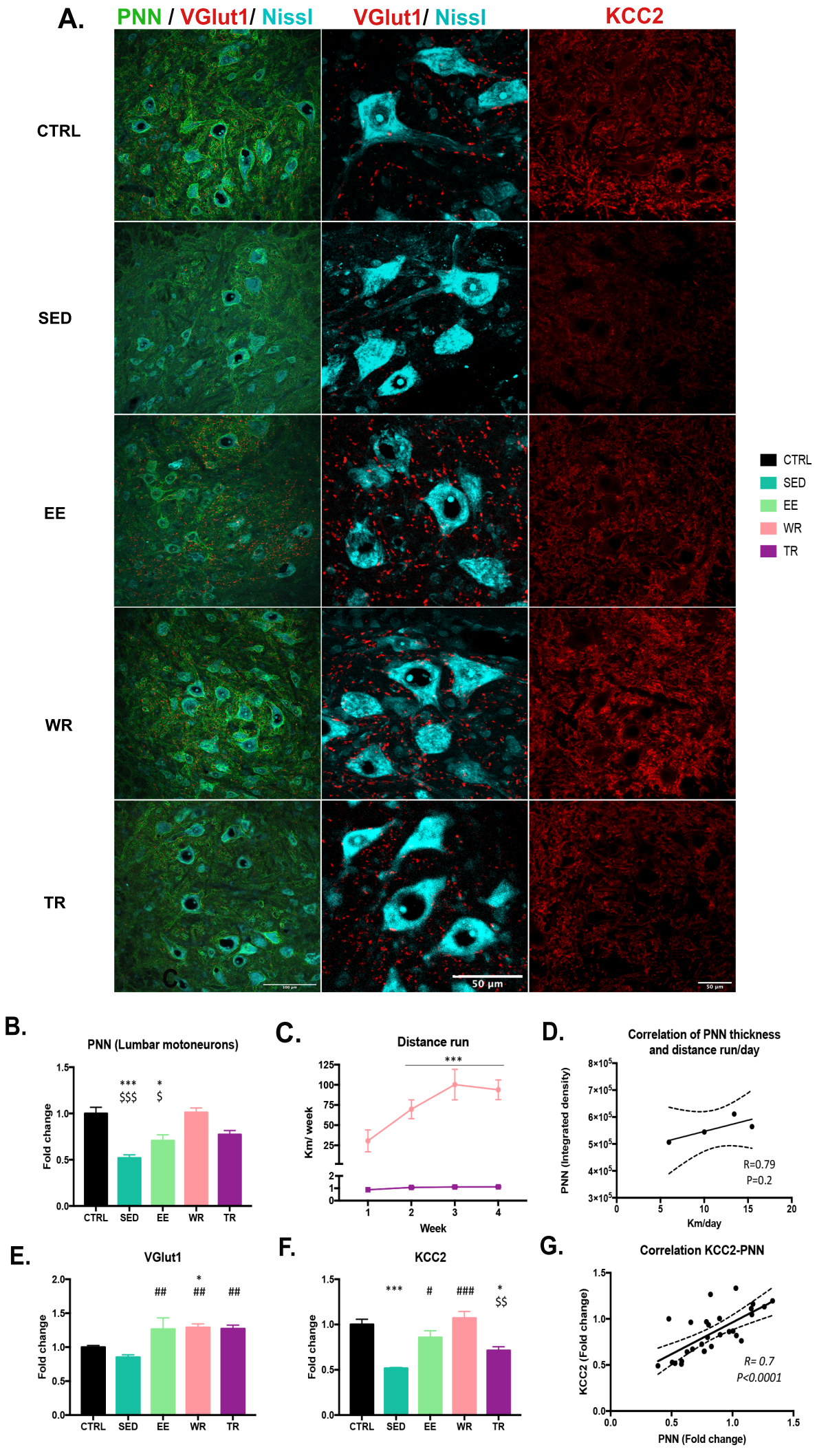
A.
PNN / VGlut1/ Nissl
VGlut1/ Nissl
KCC2
CTRL
SED
EE
WR
TR
50 µm
B.
PNN (Lumbar motoneurons)
Fold change
C.
Distance run
Km/ week
Week
D.
Correlation of PNN thickness and distance run/day
PNN (Integrated density)
Km/day
R=0.79
P=0.2
E.
VGlut1
Fold change
F.
KCC2
Fold change
G.
Correlation KCC2-PNN
KCC2 (Fold change)
PNN (Fold change)
R= 0.7
P<0.0001

# Figure 4

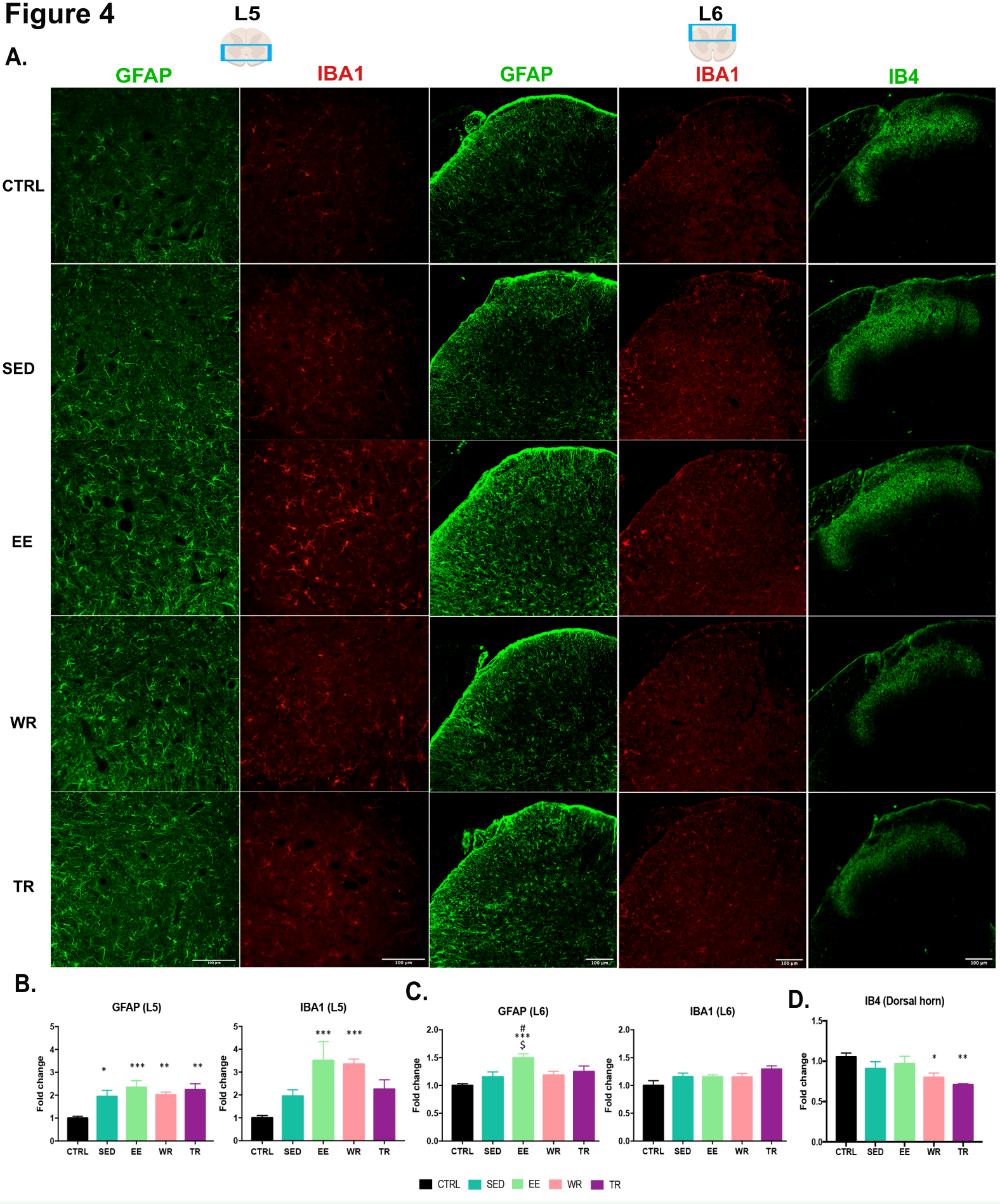
A.
L5
L6
GFAP
IBA1
GFAP
IBA1
IB4
CTRL
SED
EE
WR
TR
B.
GFAP (L5)
IBA1 (L5)
C.
GFAP (L6)
IBA1 (L6)
D.
IB4 (Dorsal horn)
Fold change
CTRL
SED
EE
WR
TR

# Figure 5

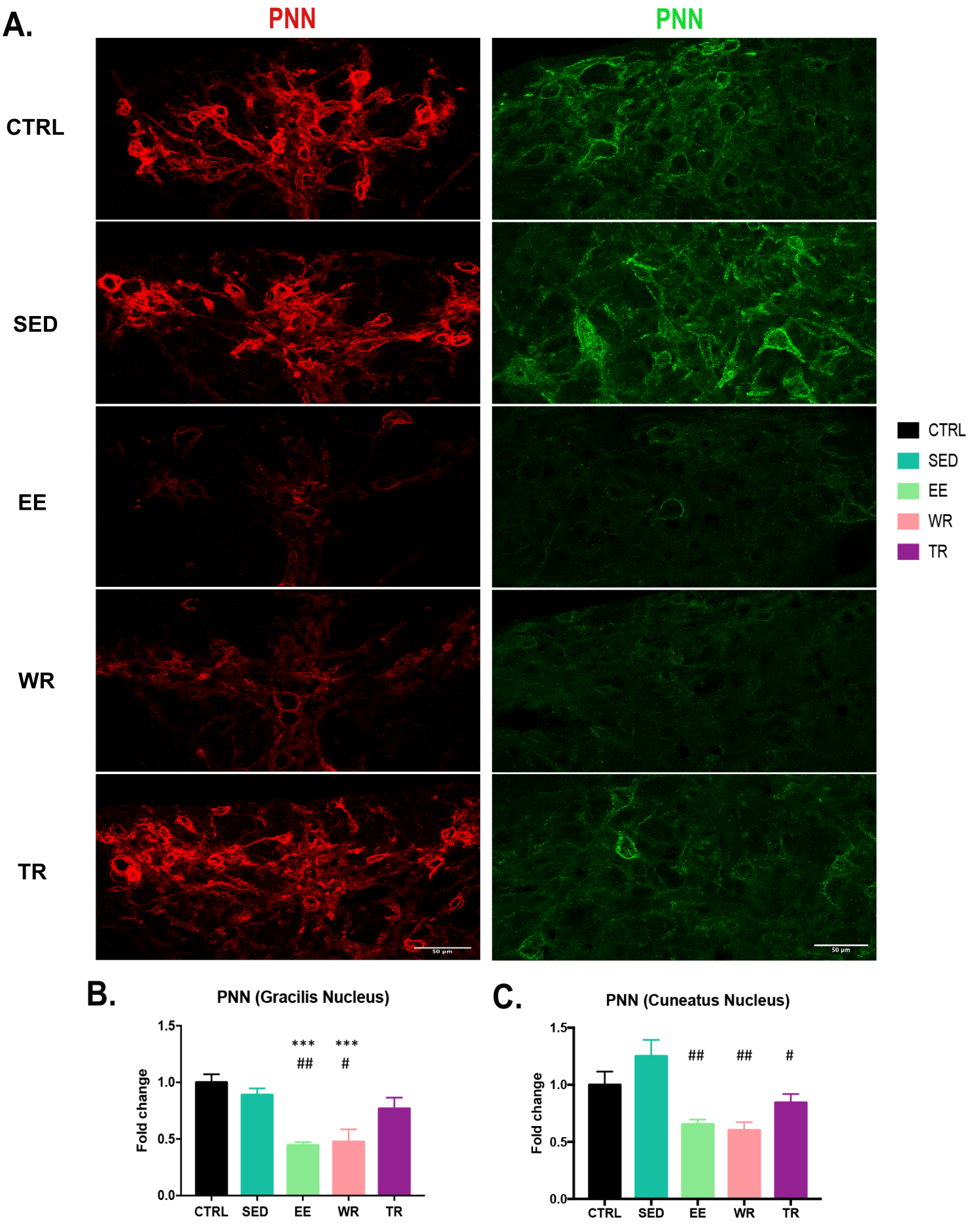
A.
PNN
PNN
CTRL
SED
EE
WR
TR
50 µm
50 µm
CTRL
SED
EE
WR
TR
B.
PNN (Gracilis Nucleus)
Fold change
1.5
1.0
0.5
0.0
*** ***
## #
CTRL SED EE WR TR
C.
PNN (Cuneatus Nucleus)
Fold change
1.5
1.0
0.5
0.0
## ## #
CTRL SED EE WR TR

Figure supplementary 1

# Figure Supplementary 1

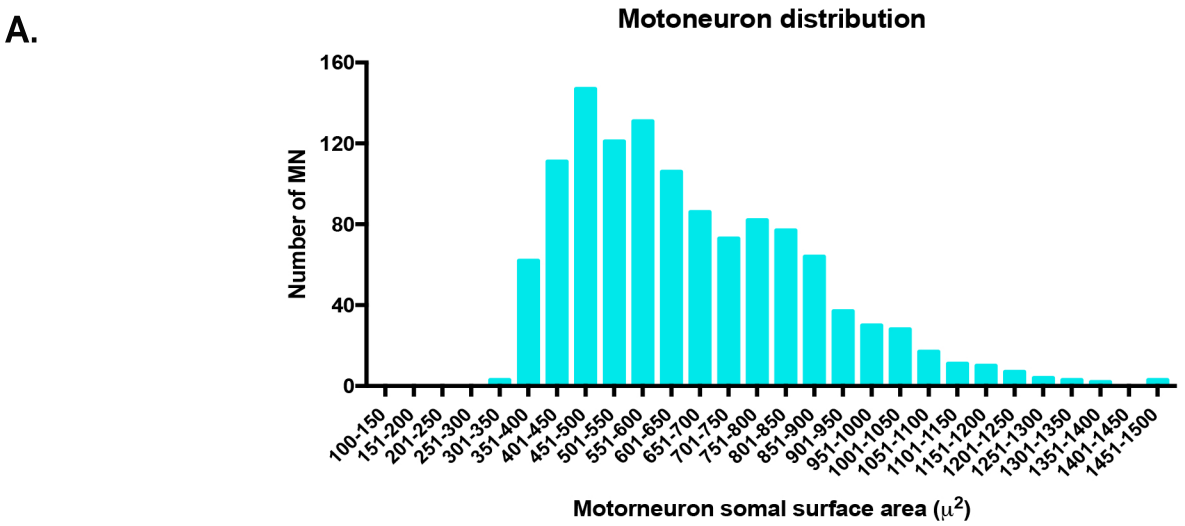


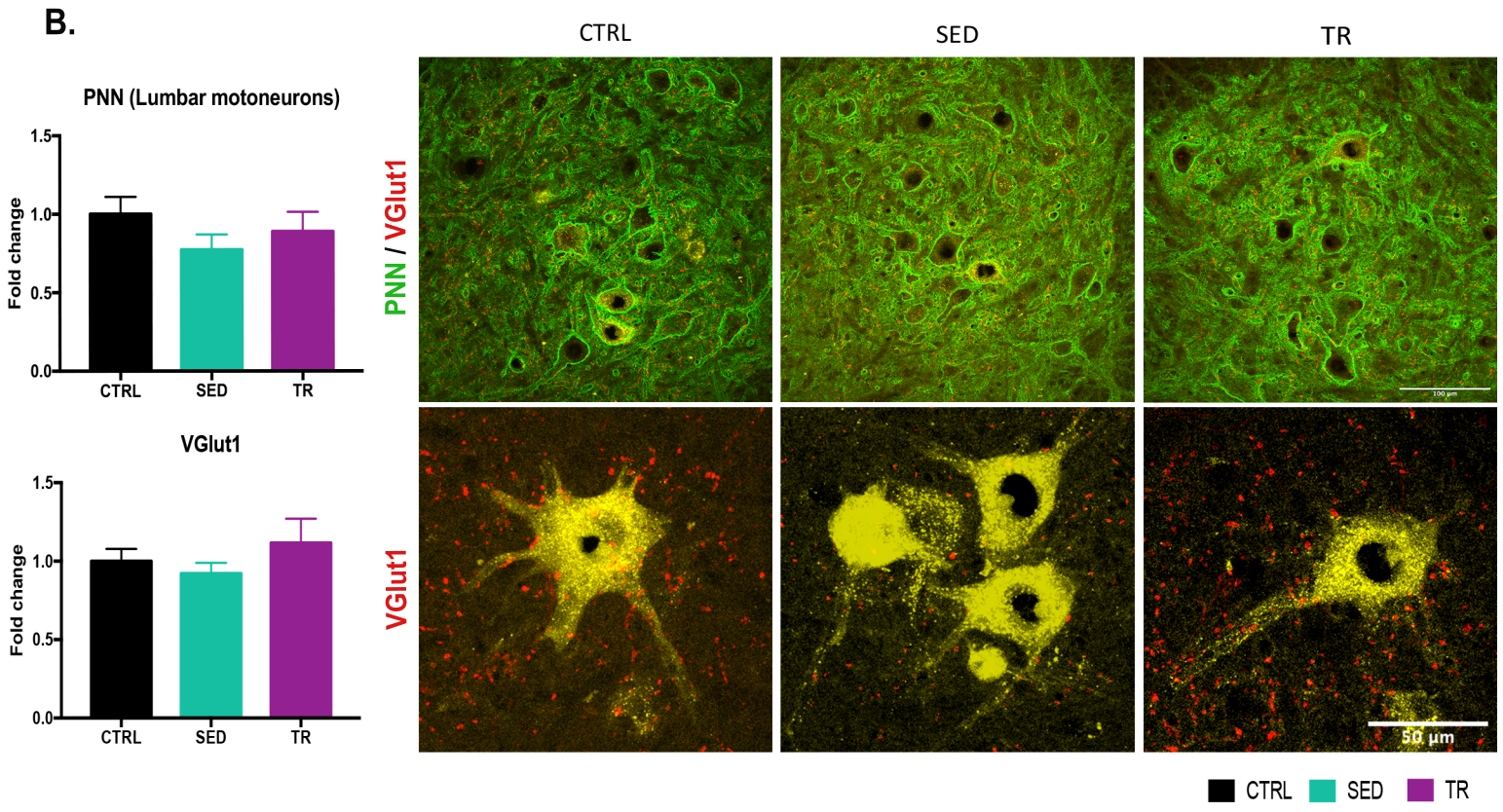

Figure supplementary 2
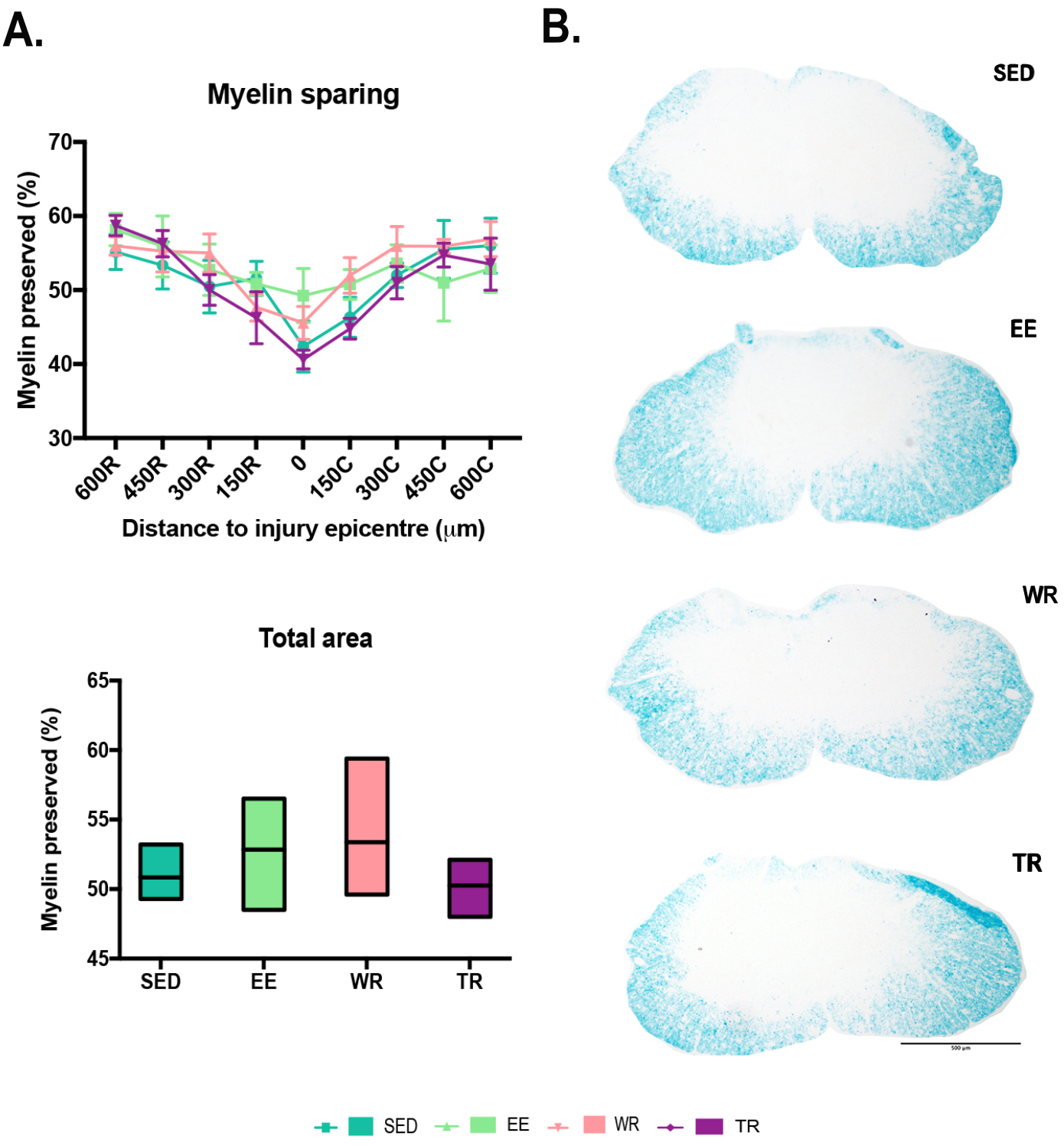
# Figure Supplementary 2